Chemical Geology 265 (2009) 122–133

Contents lists available at ScienceDirect

Chemical Geology

journal homepage: www.elsevier.com/locate/chemgeo

Geochemical effects of CO_2 sequestration on fractured wellbore cement at the cement/caprock interface

Marcus Wigand [a,*], John P. Kaszuba [b,1], J. William Carey [b], W. Kirk Hollis [a]

[a] Chemical Sciences and Engineering (C-CSE), Los Alamos National Laboratory, Los Alamos, New Mexico 87545, USA
[b] Earth and Environmental Sciences (EES-6), Los Alamos National Laboratory, Los Alamos, New Mexico 87545, USA

ARTICLE INFO

Article history:
Accepted 14 April 2009

Keywords:
Carbon sequestration
Geochemistry
Wellbore cement
Caprock
Carbon dioxide
Alteration

ABSTRACT

The potential impact to the integrity of wellbore cements as a result of exposure to supercritical carbon dioxide ($SCCO_2$) has been raised as an area of some concern with respect to long-term effectiveness of CO_2 storage in geological formations. In flow-through experiments we simulated diffusion of brine and $SCCO_2$ from the interface between wellbore cement and caprock into a fracture-bearing Portland cement. The experiments were performed at *in-situ* reservoir pressure (pore pressure: 19.9 MPa) and temperature (54 °C) conditions for 113 days. For this purpose we saturated illite-rich shale and the Portland cement core (2.02 cm × 5.35 cm) with 1.65 M brine for 14 days. After this period of time we injected $SCCO_2$ into the system for 99 days and simulated a diffusion process by using a pressure gradient of 0.7 MPa. Calcite precipitation occurred within the fracture and the induced pressure of crystal growth may explain an increase in the relative permeability along the fracture with time. $SCCO_2$-induced reactions extended ~5 mm into the Portland cement core from the fracture and formed an orange-colored zone. The orange-colored zone is nearly completely carbonated with crystalline phases consisting mainly of calcite, aragonite, and vaterite. The only crystalline cement component that persisted in the orange-colored zone was brownmillerite. Interior portions of the hydrated cement were partially carbonated, modified in texture and contained newly formed calcite, hydrogarnet and hydrocalumite (Friedel's salt). Cement porosity decreased from 37.8% to 23.8% during carbonation and was associated with a 19.6% increase in mass.

1. Introduction

Greenhouse gas emissions from combustion of fossil fuels are very likely responsible for the increase of atmospheric carbon dioxide (CO_2) concentrations from pre-industrial levels of 280 ppm (parts per million) to present levels of 375 ppm. Increased atmospheric CO_2 is thought to be the main driving factor of climate change (e.g., Karl and Trenberth, 2003). Geological storage of CO_2 in deep saline aquifers and depleted oil/gas reservoirs has the potential to reduce the release of greenhouse gases while still allowing for the use of fossil fuels (e.g., Pacala and Socolow, 2004). Thus, the development and wide deployment of cost-effective CO_2 capture and storage technology can contribute significantly to sustainable economic development. The main barriers for implementing geological storage of greenhouse gases are the additional costs arising from CO_2 capture and transport and the need to prove the reliability of the reservoir seals for relevant space and time scales. An issue critical to reservoir integrity is the potential migration of CO_2 through sealing formations via pathways formed by reactions of supercritical carbon dioxide ($SCCO_2$) with either the caprock or the wellbore, specifically the wellbore cements.

Portland cement is usually used as a sealing material for wellbores. It contains hydrated cement phases, such as portlandite and calcium silicate hydrates (C-S-H), which readily react with $SCCO_2$ to form calcite, dolomite, and amorphous silica gel (e.g., Short et al., 2001; Jacquemet et al., 2005; Regnault et al., 2005). Changes in porosity, density and texture due to this carbonation may impact mechanical and hydrologic properties of the wellbore cement (Carey et al., 2007).

CO_2 migration and carbonation in defect-free cement is likely to be a relatively slow process because of the low permeability and capillary properties of Portland cement (Carey et al., 2007; Kutchko et al., 2007). A greater concern is the possibility that CO_2 may exploit defects such as fractures that may exist in the cement sheath. These fractures may develop because of changes of pressure and temperature within the wellbore during field operations, e.g., overpressure during the injection of $SCCO_2$. Other processes that may lead to fractures and defects include cement shrinkage during hydration, mechanical shock from pipe tripping, poor cement slurry placement and residues of drilling mud and drill cuttings. These defects may provide an initial higher permeability pathway for CO_2. The question of whether these

* Corresponding author. Now at Production Engineering and Well Productivity (PEWP), Chevron Energy Technology Company, Houston, Texas 77002, USA. Tel.: +1 832 854 4229; fax: +1 832 854 7900.
E-mail address: MWJM@chevron.com (M. Wigand).
[1] Now at Department of Geology & Geophysics & School of Energy Resources, University of Wyoming, Laramie, Wyoming 82071 USA.

0009-2541/$ – see front matter © 2009 Elsevier B.V. All rights reserved.
doi:10.1016/j.chemgeo.2009.04.008

pathways will deteriorate with $SCCO_2$ flow (due to cement dissolution) or will be self-sealing (due to carbonate precipitation) is important to evaluating the long-term potential for migration of CO_2 through the wellbore annulus into overlying rocks or to the surface.

An excellent field site for studies of the long-term behavior of wellbore cement in a CO_2-rich environment is the SACROC Unit, a CO_2-enhanced recovery oil reservoir located in the eastern portion of the Horseshoe Atoll (Permian Basin, Western Texas; e.g., Carey et al., 2007). SACROC is operated by Kinder Morgan CO_2 Company and occupies 210 km^2 with 1800 wells. CO_2-flooding activities began in 1972, making SACROC the oldest, continuously operated, enhanced oil recovery operation in the United States.

Carey et al. (2007) described the alteration of a sample of 50 year-old wellbore cement from a well with nearly 30 years exposure to $SCCO_2$. The CO_2 was able to intrude the wellbore cement between 0.1 and 1 cm and the Portland-based cement was altered at the cement–caprock interface, forming a distinctive orange-colored carbonation zone. Although Carey et al. (2007) identified the reactions responsible for the alteration and estimated a time span of about 30 years for the partially carbonation of the wellbore cement, they were not able to quantify the amount of CO_2 that generated these reactions.

In this experimental study we focus on geochemical reactions and mass transfer processes that occur during $SCCO_2$ flow along a preexisting cement fracture. The design of the experiment allows us to simulate flow of a brine and $SCCO_2$ mixture from shale into cement at the caprock/cement interface. Experimental pressure, temperature and fluid composition were chosen to emulate field conditions of the SACROC Unit and the validity of our experimental results is compared to actual cement carbonation processes observed in this context.

2. Materials and methods

2.1. Experimental apparatus

The experiment was conducted in a flow-through apparatus manufactured by Coretest Systems, Inc. A Hassler core holder was used to place a confining stress around the radial axes of the cylindrical core, thus simulating lithostatic pressure and avoiding flow of injected fluids along the interface between sleeve and core sample. A schematic of the core flooding apparatus with the experimental setup is shown in Fig. 1. The fluids are injected into the system using high pressure syringe pumps (ISCO 500D) manufactured by Teledyne ISCO. System pressure was maintained by a backpressure regulator (BPR) at the core outlet that works by an inert gas over fluid technique.

2.2. Analytical techniques

Major and trace element abundances of the mineral phases (Table 1) were determined by X-ray fluorescence (XRF). Selected trace elements (Mo, Be, As, Pb, Hg, U, Th, Tl, Cu, Sb, Li, And Cs) were analyzed using inductively coupled plasma mass spectrometry (ICP-MS; Perkin Elmer Sciex Elan 6100). EPA (Environmental Protection Agency) method 3052 (i.e., microwave assisted digestion of siliceous and organically based matrices) was used to digest the shale and cement for trace element analysis. H_2O and CO_2 contents were analyzed by thermogravimetric analysis with a mass spectrometer (TGA-MS; NETSCH STA 409-CD). The samples were first dried in a vacuum oven at 110 °C for 24 h. Initial sample weight at room temperature was then measured and changes in sample weight (losses or gains) were continuously monitored as temperature was increased from room temperature to 1200 °C at 10 °C·min^{-1} in a He atmosphere. Weight loss events were assigned to H_2O and CO_2 bearing cement phases. The results of the TGA-MS analysis were also used in combination with X-ray diffraction (XRD) and scanning electron microscopy (SEM) with an energy dispersive X-ray spectroscopy system (EDX) to identify mineral phases. Additionally, laser ablation inductively coupled plasma mass spectrometer analysis (LA-ICP-MS) was performed to determine the distribution of selected major and trace elements. Porosities were determined using a conventional He-pycnometer technique. Before measuring the porosity, the cement cylinder (2.02 cm × 5.35 cm) was dried in a vacuum oven at 110 °C for 72 h. Samples masses were determined using a standard scale accurate to 1 μg.

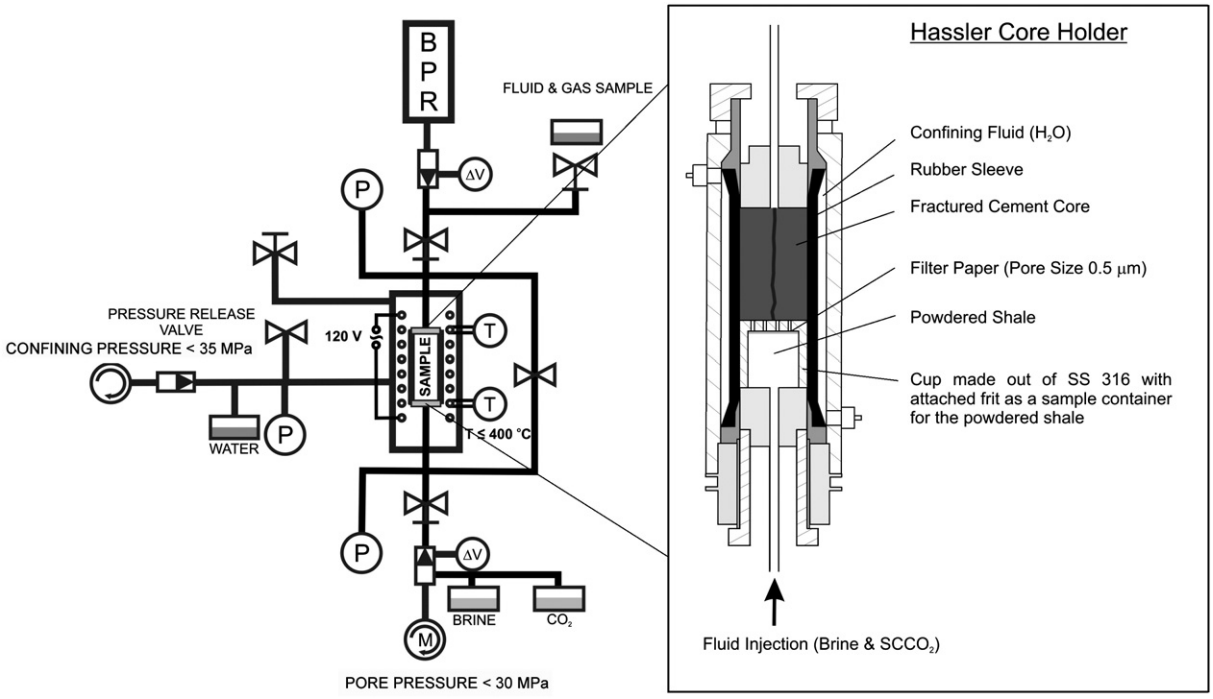

Fig. 1. Schematic of the core flooding apparatus with the experimental setup. (BPR, P, M, T, V stand for back pressure regulator, pressure transducer, DC servo motor-driven syringe pump, thermocouple, and mass flow controller, respectively).

Table 1
Major and trace element chemistry and mineralogy of the illite-rich shale and Portland cement before and after the experiment.

	U2-E1-IS	U3-E1-S1	U3-E1-PC	U3-E1-OZ	U3-E1-GZ	Upper continental crust
	Initial shale	Shale after experiment	Portland cement before experiment	Orange zone	Gray zone	
(wt.%)						
SiO_2	58.7 ± 0.8	56.6 ± 0.8	16.4 ± 1.2	13.5 ± 1.2	17.2 ± 1.2	65.9
TiO_2	0.65 ± 0.02	0.61 ± 0.01	0.15 ± 0.01	0.12 ± 0.01	0.15 ± 0.01	0.50
Al_2O_3	13.0 ± 0.3	12.5 ± 0.8	3.80 ± 0.51	3.07 ± 0.54	3.92 ± 0.51	15.2
$Fe_2O_{3\ tot}$	4.38 ± 0.06	4.26 ± 0.06	2.68 ± 0.05	2.17 ± 0.05	2.79 ± 0.05	4.99
MnO	0.03 ± 0.01	0.06 ± 0.01	0.04 ± 0.01	0.03 ± 0.01	0.04 ± 0.01	0.07
MgO	2.29 ± 0.06	2.16 ± 0.06	1.51 ± 0.06	1.15 ± 0.05	1.56 ± 0.06	2.20
CaO	4.88 ± 0.08	4.95 ± 0.08	51.7 ± 0.4	42.2 ± 0.3	53.4 ± 0.4	4.19
Na_2O	1.05 ± 0.08	2.65 ± 0.07	0.17 ± 0.10	0.32 ± 0.10	b.d.l.	3.89
K_2O	2.92 ± 0.06	2.76 ± 0.06	0.54 ± 0.03	0.63 ± 0.03	0.05 ± 0.04	3.39
P_2O_5	0.10 ± 0.01	0.10 ± 0.01	0.14 ± 0.01	0.11 ± 0.01	0.15 ± 0.01	0.20
H_2O^+	–	–	18.6	0.01	14.7	–
CO_2	–	–	2.92	36.6	4.71	–
LOI	11.13	12.80	–	–	–	–
SUM	99.16	99.52	98.69	99.90	98.69	100.53
(ppm)						
V	101 ± 17	91 ± 16	44 ± 14	30 ± 13	47 ± 14	107
Cr	149 ± 12	160 ± 12	b.d.l.	b.d.l.	11 ± 10	85
Ni	73 ± 7	74 ± 7	b.d.l.	7 ± 4	b.d.l.	44
Zn	132 ± 13	121 ± 13	89 ± 13	78 ± 12	78 ± 13	71
Rb	135 ± 9	126 ± 8	29 ± 5	32 ± 5	b.d.l.	112
Sr	145 ± 11	131 ± 10	620 ± 29	524 ± 26	644 ± 30	350
Y	18 ± 8	25 ± 8	21 ± 6	b.d.l.	12 ± 6	22
Zr	147 ± 10	141 ± 10	76 ± 13	58 ± 12	76 ± 14	190
Nb	16 ± 6	13 ± 7	11 ± 6	b.d.l.	16 ± 6	12
Ba	229 ± 26	214 ± 26	50 ± 26	55 ± 25	77 ± 26	550
Mo	1.55 ± 0.15	1.44 ± 0.14	–	–	–	1.5
Be	1.82 ± 0.18	2.02 ± 0.20	–	–	–	3
As	11.4 ± 1.1	10.9 ± 0.9	–	–	–	1.5
Pb	19.1 ± 1.9	20 ± 1.9	–	–	–	17
Hg	0.66 ± 0.07	0.64 ± 0.07	–	–	–	–
U	4.38 ± 0.40	4.37 ± 0.40	–	–	–	2.8
Th	10.2 ± 1.0	0.98 ± 0.10	–	–	–	10.7
Tl	1.02 ± 0.07	b.d.l.	–	–	–	0.75
Cu	35.5 ± 3.1	21.5 ± 1.9	–	–	–	25
Sb	1.24 ± 0.11	1.20 ± 0.10	–	–	–	0.2
Li	59.7 ± 5.6	41.5 ± 4.0	–	–	–	20
Cs	5.77 ± 0.53	3.35 ± 0.34	–	–	–	4.6
g	–	–	1.54	2.00	1.71	–
Φ (%)	–	–	37.77	23.80	–	–
(wt.%)						
Quartz	27.4 ± 0.6	27.5 ± 0.6	–	–	–	–
Calcite	6.2 ± 0.3	4.3 ± 0.3	3.4 ± 0.3	42.6 ± 0.9	5.4 ± 0.4	–
Aragonite			–	0.4 ± 0.1	–	–
Vaterite			–	8.5 ± 0.4	–	–
Illite	50.4 ± 0.8	51.2 ± 0.9	–	–	–	–
Pyrite	2.2 ± 0.2	2.1 ± 0.2	–	–	–	–
Albite	4.9 ± 0.4	4.6 ± 0.4	–	–	–	–
Kaolinite	1.6 ± 0.2	2.4 ± 0.2	–	–	–	–
Chlorite	0.2 ± 0.1	0.4 ± 0.1	–	–	–	–
Mica	3.9 ± 0.3	3.9 ± 0.3	–	–	–	–
Dolomite	1.6 ± 0.2	1.8 ± 0.2	–	–	–	–
Analcime	1.5 ± 0.2	1.5 ± 0.2	–	–	–	–
Halite	–	0.4 ± 0.1	–	–	–	–
Portlandite	–	–	15.9 ± 0.9	–	13.3 ± 0.6	–
Belite	–	–	4.2 ± 0.4	–	2.5 ± 0.3	–
Alite	–	–	1.5 ± 0.2	–	1.1 ± 0.2	–
Brownmillerite	–	–	0.5 ± 0.1	0.4 ± 0.1	0.4 ± 0.1	–
Katoite	–	–	0.4 ± 0.1	–	0.8 ± 0.1	–
Ettringite	–	–	0.5 ± 0.2	–	–	–
Hydrocalumite	–	–	1.0 ± 0.1	–	0.6 ± 0.1	–
Amorphous	–	–	72.7 ± 1.0	48.1 ± 1.0	75.9 ± 0.9	–
Total	100.0	100.0	100.0	100.0	100.0	–

Major and trace element concentration were measured using XRF and ICP-MS. H_2O^+ and CO_2 contents were analyzed using TGA-MS (thermogravimetric analysis) Quantitative mineral compositions were determined by XRD using 20 wt.% corundum as an internal standard. XRD results are normalized to 100% on corundum-free basis. Alite: Ca_3SiO_5; belite: Ca_2SiO_4; brownmillerite: $Ca_4Al_2Fe_2O_{10}$; katoite: $Ca_3(Al,Fe)_2(OH)_{12}$. b.d.l.: below detection limit; – : not measured. Analytical uncertainties are 2σ. g = specific gravity (g/cm^3). Φ = porosity (%). H_2O^+ represents water present in combined state within the rock or cement in hydrous minerals (e.g., illite, kaolinite, chlorite, mica, and portlandite). LOI: loss on ignition. The composition of the upper continental crust is based on Taylor and McLennan (1985, 1995).

The experiment was not designed to produce the volume of aqueous fluid needed for periodic sampling during the experiment. Instead, porewaters from the shale were recovered post-experiment by separation in a centrifuge. The mixture of shale powder and pore fluid was centrifuged for 30 min at 2700 ×g. A total of 9.2 g of fluid was recovered from the shale. This fluid was divided into subequal

Table 2
Composition of initial brine injected into the experimental system and porewater brine recovered from powdered shale.

	Units	Starting brine		Porewater extracted from shale	
Alkalinity	mM as $CaCO_3$	1.22		3.83	
Al	μM	3.00	(0.02)	112	(2)
$As(OH)_4^-$	μM	0.7	(0.1)	0.75	(0.20)
$B(OH)_3$	μM	4.0	(0.3)	216	(4)
Ba	μM	0.300	(0.002)	12.1	(2.0)
Br	mM	0.335	(0.017)	0.386	(0.019)
Ca	mM	106.9	(1.6)	75.20	(0.35)
Cl	M	1.509	(0.075)	1.473	(0.074)
Cr	μM	0.90	(0.01)	3.4	(0.5)
Cs	μM	<0.2		1.0	(0.2)
Cu	μM	9.7	(0.2)	26	(10)
Fe	μM	0.70	(0.03)	221	(3)
K	mM	0.421	(0.003)	36.37	(0.58)
Li	μM	2.00	(0.03)	240	(58)
Mg	mM	29.8	(0.3)	88.89	(0.73)
Mn	μM	<0.2		31.1	(0.4)
Mo	μM	<0.3		2.8	
Na	M	1.414	(0.008)	1.353	(0.005)
Ni	μM	3.20	(0.03)	95.6	(20.3)
Rb	μM	<0.4		36.1	(6.5)
Se	μM	2.60	(0.09)	2.3	(0.4)
SiO_2	mM	0.013	(0.001)	0.542	(0.012)
SO_4	mM	5.28	(0.26)	10.48	(0.52)
Sr	mM	0.0260	(0.0001)	0.245	(0.003)
Zn	μM	<0.5		3.00	(0.03)
TDS	ppm	91977		91698	
Bench pH		6.61		Not measured	
In-situ pH		4.3		4.1 to 5.0	
Charge balance		+5.2%		+6.8%	

2σ uncertainty in parentheses. *In-situ* pH calculated using Geochemist's Workbench 6.0.2 (Bethke, 2006), the thermodynamic dataset thermo.dat, and the B-dot ion association model. Calculation performed sequentially by using these tabulated chemical analyses and bench pH as input data, increasing temperature (from 25 to 54 °C), then adding alkalinity up to analyzed values. Bench pH for starting brine was measured using a glass electrode after depressurization and cooling to room temperature. The bench pH of shale porewater recovered at the end of the experiment was not measured; therefore *in-situ* pH calculations were performed assuming a range of reasonable benchtop values (pH 5 to 9). This approach yields an *in-situ* pH range of 4.1 to 5.0. Not listed and below detection levels in both brines: Ag, Be, Cd, Co, F, Hg, NO_3, Pb, PO_4, Sb, Sn, Th, Ti, Tl, U, V.

fractions for cation and anion analysis. To prevent precipitation, the aliquot of brine for cation analysis was acidified to pH 2 with nitric acid. Dissolved Si, Ca, Mg, Na, K, and B were determined by ICP-OES (Inductively Coupled Plasma Optical Emission Spectroscopy), dissolved Al, Fe, and Mn by ICP-MS, and dissolved anions by ion chromatography. Mineral precipitates were not observed in any of the samples. Analytical results and uncertainties are reported in Table 2.

2.3. Materials

Illite-rich shale of the Wolfcamp Formation (Permian Basin, West Texas) was chosen as the caprock material (Table 1). The shale consists of illite (50.4 ± 0.8 wt.%) and quartz (27.4 ± 0.6 wt.%) with lesser amounts of calcite, albite, mica, pyrite, dolomite, kaolinite, analcime, chlorite, and organic material which occurs between the clay layers. The shale is fossiliferous and the clay layers are rich in dark-brown organic material. In thin-sections cut parallel to the bedding, fossils and mud clast textures are evident. The SiO_2 concentration of the illite-rich shale is within typical upper crust abundances (Table 1; Taylor and McLennan, 1985, 1995). Major elements such as Ti and Ca are slightly enriched and Al and Na slightly depleted compared to the average upper continental crust. The incompatible trace element characteristics normalized to the upper continental crust (Taylor and McLennan, 1985, 1995) are shown in a spider diagram (Fig. 2). Compared to average concentrations of the upper continental crust, unreacted shale (U3-E1-IS) is enriched in Cs, Rb and U and depleted in Ba, K, La, Ce, Sr, Nd, Zr, Sm, Y, and Yb.

The cement paste was made from API (American Petroleum Institute) class G Portland well cement and tap water with a water–cement ratio of 0.4 by mass. This mixture was transferred to a container and cured for 122 days at room temperature. A cement cylinder with a diameter of 2.02 cm and a length of 5.35 cm was drilled out of the solidified block using a diamond core drilling bit. A hammer and chisel were used to produce a fracture with a rough-textured surface down the longitudinal axis of the cement cylinder. The mineral composition (Table 1) indicates that even after 122 days the cement paste was not completely hydrated because cement phases such as alite (Ca_3SiO_5), belite (Ca_2SiO_4), and brownmillerite ($Ca_4Al_2Fe_2O_{10}$) were still present. Portlandite ($Ca(OH)_2$; Fig. 3A) is the predominant crystalline hydrated cement phase (15.9 ± 0.9 wt.%) followed by 1.0 ± 0.1 wt.% hydrocalumite ($Ca_2Al(OH)_6[Cl_{1-x}(OH)_x]\cdot 3(H_2O)$), 0.5 ± 0.2 wt.% ettringite ($Ca_6Al_2(SiO_4)_3(OH)_{12}\cdot 26(H_2O)$) (Fig. 3B), and katoite ($Ca_3(Al,Fe)_2(OH)_{12}$). Additionally, the Portland cement contains a substantial amount of amorphous material. Due to the long curing time under air and the use of tap water for preparing the cement paste, the cured cement also contains 3.4 ± 0.3 wt.% calcite. The porosity of the dried cement cylinder, as measured before the experiment was 37.8%.

The brine used for this experiment was based on the average composition of brines collected from the Cisco and Canyon Formations of the Permian Basin, West Texas. The average composition of the brine was calculated from 100 selected analyses (charge balance within 2%) of the NETL database (Table 2; National Energy Technology Laboratory, 2002).

2.4. Experimental procedure

The experiment was conducted at 54 °C with a pore pressure of 19.9 MPa and a confining pressure of 26.2 MPa. A composite consisting of the dry cement cylinder and a 3.2 cm thick layer of powdered shale separated by a stainless-steel frit was mounted into the Hassler core holder, pressurized, and saturated with 1.65 M brine (Table 2) over an initial soak period of 174 h. The orientation of the Hassler core holder was vertical during the experiment and the fluids were injected first into the shale and then flowed into the cement core. The $SCCO_2$ will migrate through the brine and will be H_2O-saturated at the shale/cement interface.

The experiment was conducted in four stages with different pressure gradients. Fig. 4 shows the evolution of head pressure P_H, back pressure P_B, and pressure gradient ΔP over time. In the initial soak period, the back pressure was set to approximately zero

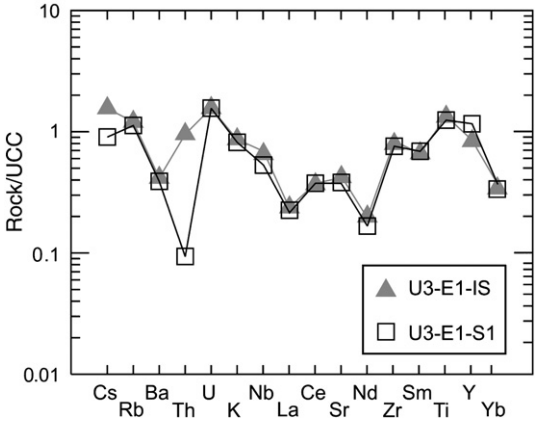

Fig. 2. Upper continental crust (UCC) normalized multi element diagram for the illite-rich shale of Wolfcampian age (U3-E1-IS; shale before the experiment) and the shale after the experiment (U3-E1-S1). Normalizing UCC values are after Taylor and McLennan (1985, 1995).

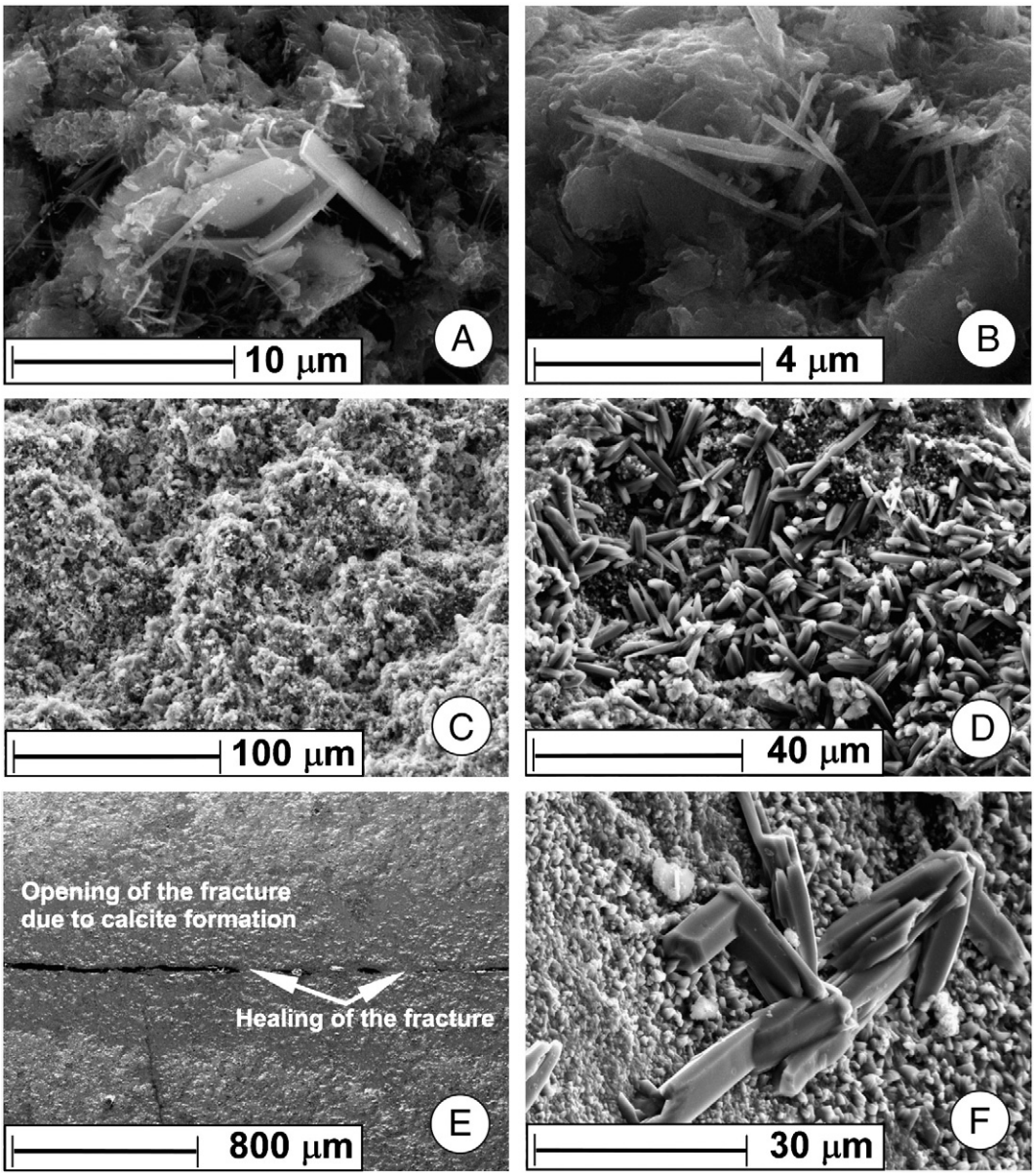

Fig. 3. Secondary electron (SE) and backscattered electron (BSE) micrographs of selected areas of the cement core before and after the reaction with the mixture of brine and $SCCO_2$. (A): Idiomorphic portlandite crystals surrounded by ettringite and calcium silicate hydrates; (B): Ettringite fibers; (C): Surface of the fracture before the experiment; (D): Surface of the fracture after the experiment; (E) Cross section of the fracture after the experiment; (3F): Calcite crystals inside a pore of the orange zone.

(producing the maximum available pressure gradient) to ensure that the shale and the core were completely saturated with brine. The total amount of brine injected into the system was 26.47 ml. Over that time span the back pressure remained near 0 MPa indicating that there was little flow of brine along the fracture or through the cement. The impermeability of the fracture may have been a result of the 26.2 MPa confining pressure applied to the core.

After the initial brine–saturation stage, the back pressure was increased to create a pressure gradient (ΔP) of 1.1 MPa and injection of $SCCO_2$ under constant pressure (19.9 MPa) was begun. The low pressure gradient was designed to simulate a diffusion process of H_2O saturated $SCCO_2$ from the chamber filled with powdered caprock into the cement. The injection of $SCCO_2$ into the system was performed over 980.92 h during which the back pressure gradually increased to an equilibrium state (i.e., P_H–P_B). An average flow rate of 0.0015 ml·min^{-1} (88.3 ml in total) was observed during this injection phase.

In the third stage of the experiment, the back pressure was decreased to 12.9 MPa for a pressure gradient of ~6.9 MPa and the injection of $SCCO_2$ was started again. The average flow rate increased during the second saturation phase to a value of 0.0023 ml·min^{-1}. To further investigate the flow characteristics of H_2O saturated $SCCO_2$ along a cement fracture the same procedure was repeated again in a fourth stage and yielded a further increase of the average flow rate to 0.0043 ml·min^{-1}.

3. Results

3.1. Changes in the mineralogy of the Portland cement

Reaction of Portland cement with brine and $SCCO_2$ formed two distinct regions separated by a narrow transition zone (Fig. 5). An orange-colored zone was formed in the cement due to the reaction with H_2O saturated $SCCO_2$, displaying an average thickness of ~0.6 cm. The orange-colored zone contains three polymorphs of $CaCO_3$: calcite (42.6 ± 0.9 wt.%), aragonite (0.4 ± 0.1 wt.%), and vaterite (8.5 ± 0.4 wt.%) (Table 1). Idiomorphic calcite crystals occur within larger pores inside the orange-

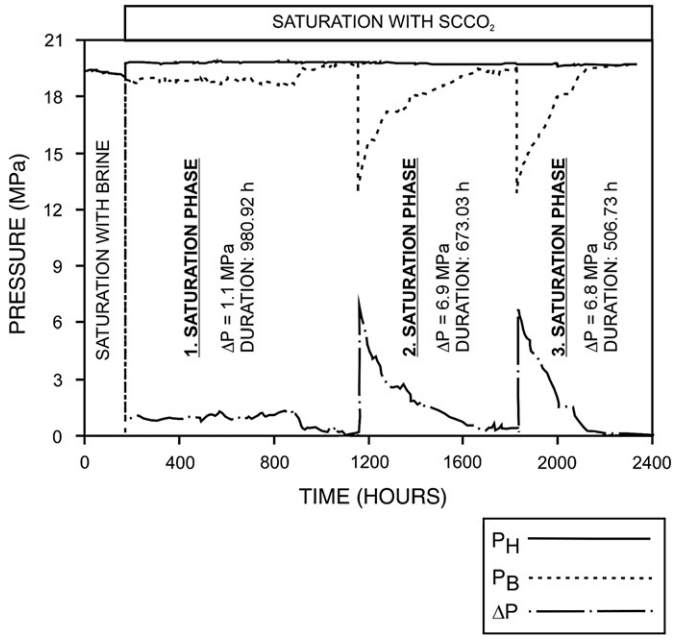

Fig. 4. Time versus pressure diagram indicating the experimental history. The diagram includes the head pressure (P_H) and the back pressure (P_B) measured on both ends of the sample. The pressure difference ΔP was calculated as $P_H - P_B$. In the first phase of the experiment (174 h), brine was injected with $P_B = 0$. In the subsequent three saturation phases, CO_2 was injected with initial P_B varying between 18.9 and 12.9 MPa.

colored zone (Fig. 3F). The only original, crystalline cement phase which persisted in the orange zone following reaction with $SCCO_2$ and brine was brownmillerite.

The gray-colored zone has an average thickness of ~1.5 cm and is separated from the orange-colored zone by a ~100 μm width dark gray zone (transition zone; Fig. 5). The gray-colored zone is partially carbonated (5.4 ± 0.4 wt.% calcite) but the presence of the highly reactive hydrated cement phases portlandite and hydrogarnet suggests that reaction with H_2O saturated $SCCO_2$ was not as extensive as in the orange-colored zone. In contrast to the orange-colored zone the carbonation process in the gray-colored zone produced only calcite. The cement phases alite, belite and brownmillerite are still present in the gray-colored zone. Compared to the original Portland cement the amount of alite and belite decreased whereas the amount of hydrogarnet and amorphous material increased during the experiment (Table 1). The amount of other hydrated cement phases such as portlandite and hydrocalumite also decreased in the gray zone.

At both surfaces of the fracture we observed growth of abundant idiomorphic calcite crystals and a related change in texture of the cement (Fig. 3D). The surface structure inside the fracture before the experiment (Fig. 3C) shows the typical cement texture including cement phases such as fibrous calcium silicate hydrates (C-S-H) and hexagonal plates of portlandite. Fig. 3E shows a SEM micrograph (in backscattered electron mode, BSE) of a cross section of the altered cement core with the fracture oriented horizontally. Measurements along the fracture yielded an opening from ≤2.8 μm to ≤56.7 μm width that appeared to show both a widening in some places and a partial healing of the fracture. A compact carpet of idiomorphic to hypidiomorphic calcite crystals (~1500 calcite crystals with an average volume of 248.8 μm^3 per mm^2) was formed on each side of the fracture due to the carbonation process and may have led to opening of the fracture (Fig. 3E).

3.2. Fluid chemistry

Injection of $SCCO_2$ into the experiment produced significant changes in the brine recovered from the shale, changes that are apparent by comparing the composition of porewater brine with brine initially introduced into the powdered shale (Table 2). The concentrations of predominant brine constituents Na and Cl decreased by 4.3 and 2.4%, respectively, and Ca concentrations decreased by 29.7% to 75 mM. Total dissolved solids and the trace metals As, Br, and Se remain relatively unchanged whereas concentrations of all other brine constituents increased in the shale porewater relative to the starting brine: Al, $B(OH)_3$, Fe, K, and Li by 40 to 300×; Ba, SiO_2, Ni and Sr by 10 to 40×; and Cr, Cu, Mg and SO_4 by 2 to 4×. Trace metals previously absent from starting brine appeared in porewater brine at μM quantities (Cs, Mn, Mo, Rb and Zn), possibly indicating subtle changes in the alteration mineral assemblage.

To understand changes in fluid chemistry observed in the experiment, calculations were performed with Geochemist's Workbench 6.0.2 (Bethke, 2006) using the thermodynamic dataset thermo.dat and the B-dot ion association model. *In-situ* pH of starting brine was calculated as described in Table 2, using pH measured at the bench as a starting value. The decrease between the pH value measured at the bench and the calculated *in-situ* pH is partly due to the decrease of the stability constant of H_2O (K*w*) with increasing temperature ($\Delta pH = -0.4$) and largely to increased amounts of carbonic acid dissolved in brine due to CO_2 injection ($\Delta pH = -1.9$). Since pH of porewater recovered from the shale was not measured at the bench, *in-situ* pH calculations were performed assuming a range of reasonable benchtop pH values (pH 5 to 9). This approach yields an *in-situ* pH range of 4.1 to 5.0. The significant increase in concentration of most metals and trace elements in the porewater brine suggests that the shale has dissolved by reaction with acidic brine, behavior consistent with the *in-situ* pH we have calculated. Increased SiO_2 concentrations in porewater brine relative to starting brine are significant enough to shift the saturation state of quartz from undersaturated (log saturation index = −1.16) to supersaturated (log saturation index = +0.46).

3.3. Mass transfer of the Portland cement with $SCCO_2$ and brine

Bulk compositions of the original Portland cement and the gray and orange zones that were formed during the experiment were determined by XRF and TGA-MS (Table 1). Changes in elemental concentrations between the original Portland cement (C_n^0) and the altered cement zones, (C_n^a) assuming constant volume ($F_V = 1$), were calculated using the following equation:

$$X_n^{cv}(\%) = \frac{100\left(C_n^a - C_n^0\right)}{C_n^0} \quad (1)$$

where X_n^{cv} is the percentage change in concentration of component *n* from the original Portland cement (0) to the altered cement (a). C_n^a and

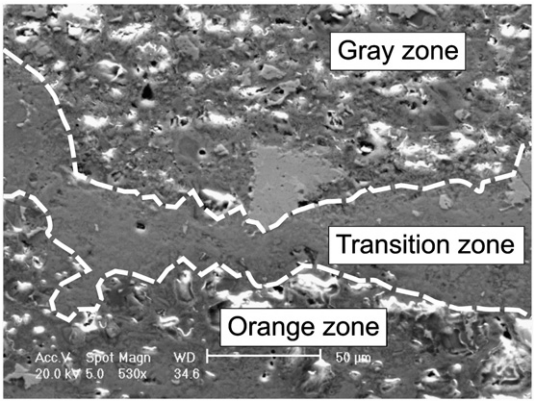

Fig. 5. BSE image of the transition zone between the orange zone and the gray zone.

C_n^0 are the concentrations of component n in the altered cement zone (a) and the Portland cement (0). The most significant changes due to the carbonation process were observed in the H_2O and CO_2 concentrations (Table 1). Whereas the original Portland cement and the gray zone contain significant H_2O amount (18.6 and 14.7 wt.%, respectively), the orange zone lost all of its structural-bond water. Water loss is due to extensive carbonation as documented by the increase in the CO_2 content from 2.92 to 36.6 wt.% in the orange zone. Following the results of Short et al. (2001), most of the structural-bond water is released to porewater by the formation of calcite from portlandite and C-S-H ($CaO{\cdot}SiO_2$) as shown in Eqs. (2)–(5).

$$Ca(OH)_2 + CO_2 + H_2O \rightarrow CaCO_3 + 2H_2O \quad (2)$$

$$3CaO{\cdot}SiO_2 + (3-x)CO_2 + yH_2O \rightarrow xCaO{\cdot}SiO_2{\cdot}yH_2O + (3-x)CaCO_3 \quad (3)$$

$$xCaO{\cdot}SiO_2{\cdot}yH_2O + xCO_2 \rightarrow SiO_2{\cdot}yH_2O + xCaCO_3 \quad (4)$$

$$3CaO{\cdot}SiO_2 + 3CO_2 + yH_2O \rightarrow SiO_2{\cdot}yH_2O + 3CaCO_3 \quad (5)$$

However, the reaction of H_2O saturated $SCCO_2$ with the gray zone resulted in a much smaller decrease in H_2O^+ and increase in CO_2 contents (Table 1) compared to the orange zone.

The percentage changes in composition for both altered cement zones, assuming constant volume and, alternatively, constant aluminum concentration (e.g., Gresens, 1967), are presented in Table 3. Reaction of Portland cement with the $SCCO_2$ and brine mixture yielded a slight enrichment in the orange zone of Na, K, and Si and larger enrichments in Ca, C and O (Table 3). In the gray zone, Si, Ca, O and C were enriched whereas Na, K, and H were slightly depleted during the alteration process.

In addition to XRF and TGA-MS analyses, LA-ICP-MS analyses were performed for a selected group of elements (Si, K, Ca, Mg, Na, Li, Rb, and U). The concentrations of these elements were normalized to the Si concentration. The results of the LA-ICP-MS analyses are shown as compositional profiles in Fig. 6. LA-ICP-MS data confirm the XRF data of enriched Na and K in the orange zone and consistency of Ca concentrations in all altered cement zones. Whereas XRF analyses suggest no changes in Mg concentrations in the different cement zones, the LA-ICP-MS profile suggests a slight Mg enrichment close to the fracture and the transition zone in the orange zone compared to the gray zone. Alkali trace elements, such as rubidium and lithium are also enriched in the orange zone and show the same behavior as Na and K. Even though U, Th, and rare earth elements (REE) are transported as carbonate complexes at low temperature in oxidizing and alkaline solutions (McLennan and Taylor, 1979), the U concentrations of the different cement zones were not affected by the reaction with the $SCCO_2$ and brine mixture.

3.4. Geochemical and mineralogical changes in the illite-rich shale (caprock)

Mineralogical changes in the illite-rich shale as determined by XRD are predominantly within analytical uncertainties. The bulk composition of the illite-rich shale before and after the experiment was determined by XRF (Table 1). Calcite was partially dissolved whereas dolomite was not affected by the $SCCO_2$ and brine mixture. There is an indication that kaolinite concentrations increased at the expense of albite due to reaction with brine and $SCCO_2$. Mineral trapping of CO_2 through formation of carbonate minerals such as dawsonite was not observed. Changes in elemental concentrations between the original shale and the altered shale, assuming constant volume, were calculated using Eq. (1). Reaction with $SCCO_2$ and brine decreased Si, Fe, Mg, and K concentrations between 1.19 and 4.35%, whereas Mn, Na, and Ni concentrations increased by 122, 156 and 4.01%, respectively. Changes in the concentrations of elements such as Ti, Al, Ca, P, V, Cr, Zn, Rb, Sr, Y, Zr, Nb, and Ba were within the analytical uncertainties. The LOI (lost on ignition) contents increased from 11.13 to 12.80 wt.% which is most likely related to the formation of clay minerals such as kaolinite.

Table 3
Weights of components (X_n) transferred into or out of the cement zones for constant volume ($F_V = 0$) and for zero change in Al ($X_{Al} = 0$).

	Orange zone	Gray zone
X_n (%) data for $F_V = 0$		
Si	+0.48	+1.25
Ti	+0.01	+0.01
Al	+0.09	+0.29
Fe	+0.09	+0.29
Mn	+0.001	+0.004
Mg	−0.01	+0.13
Ca	+2.16	+5.34
Na	+0.19	−0.12
K	+0.23	−0.40
P	±0.00	+0.01
H	−2.08	−0.26
C	+12.16	+0.63
O	+29.69	+4.18
Sum	+1.16	+6.54
Gains	+18.29	+2.06
Losses	−1.01	−2.02
Gains + losses	+17.28	+0.04
V	−6.20	+7.19
Cr	–	–
Ni	–	–
Zn	+12.21	−3.03
Rb	+11.69	–
Sr	+6.00	+9.39
Y	–	−7.94
Zr	−1.30	+8.63
Nb	–	+6.65
Ba	+21.86	+35.33
X_n (%) data for $X_{Al} = 0$		
$F_{V\,Al}$	0.96	0.88
Si	+0.153	+0.139
Ti	+0.003	±0
Al	±0	±0
Fe	+0.013	+0.019
Mn	±0	±0
Mg	−0.045	+0.002
Ca	+0.598	+0.056
Na	+0.173	−0.123
K	+0.203	−0.408
P	±0	±0
H	−2.08	−0.49
C	+11.64	+0.45
O	+26.65	−2.14
Sum	−0.97	−0.80
Gains	+17.13	+0.66
Losses	−1.06	−2.18
Gains + losses	+16.07	−1.52
V	−7.73	+0.74
Cr	–	–
Ni	–	–
Zn	+8.16	−13.77
Rb	+10.05	–
Sr	+3.28	+0.48
Y	–	−9.58
Zr	−4.29	−1.94
Nb	–	+4.51
Ba	+18.99	+24.70

–: Analyses were below detection limit. For that reason it was impossible to calculate the weights of components (X_n). The weights were rounded off to two and three decimal places respectively.

4. Discussion

4.1. Mass balance analysis

Simple inspection of elemental concentrations does not satisfactorily determine chemical exchange during cement alteration because

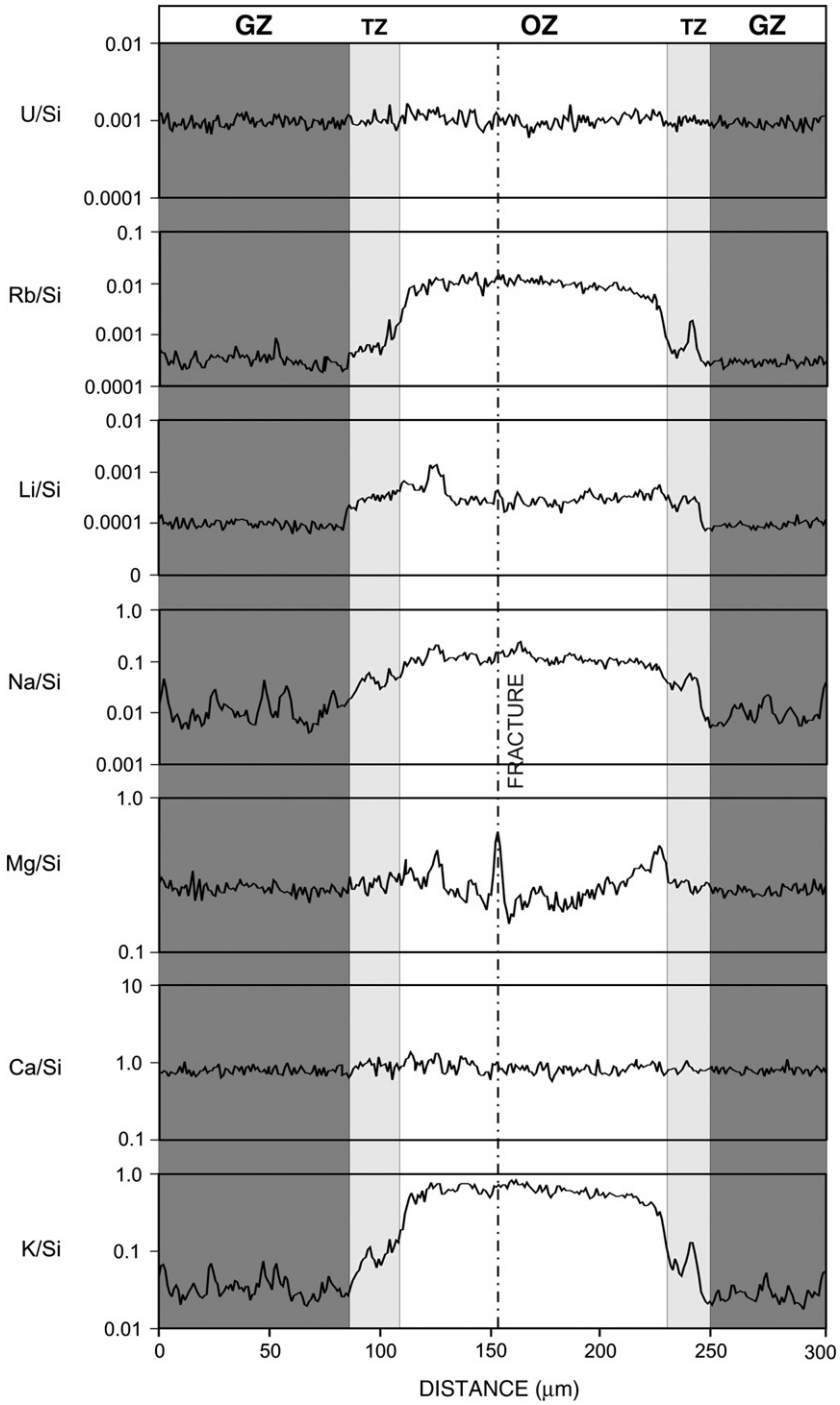

Fig. 6. LA-ICP-MS profiles for selected major and trace elements. GZ, TZ, OZ stand for gray zone, transition zone, and orange zone, respectively.

elemental concentrations are expressed as relative amounts. However, TGA-MS analyses of the different cement zones show that reaction with H_2O saturated $SCCO_2$ increased the CO_2 content (36.6 wt.%), decreased the H_2O^+ content, increased the weight and decreased the porosity of the orange zone (Table 1). The approaches of Gresens (1967) and Grant (1986) were used to quantify the gains and losses of components in the two cement zones (Table 3). Grant (1986) provides the ISOCON diagram as a simple graphical solution, in which weight percentages (m_i^a) of each element or oxide i in the altered rock are plotted versus those of unaltered rock (m_i^0). Major elements of the orange and gray zones relative to original Portland cement are compared in the ISOCON diagrams of Fig. 7A and B, respectively. The slope of the best-fit ISOCON for the immobile elements in the orange zone is 0.794. Using the measured densities, the volume (V) change associated with the alteration ($F_V = V^a/V^0 = 1.26 \times (1.54\ g \cdot cm^{-3}/2.00\ g \cdot cm^{-3})$ is 0.97, or a 3% reduction in volume. The distributions of elements in the ISOCON diagram for the orange zone (Fig. 7A) show that nearly all elements (Al, Ti, P, Si, Mg, Mn, Fe, and Ca) are relatively immobile, whereas H content decreased and Na, K, O, and C contents increased. Thus the carbonation process was nearly isochemical and isovolumetric with the replacement of H_2O by CO_2 with some addition of alkalis from the brine.

In contrast to the orange zone, the slope of the best-fit ISOCON for the gray zone is 1.034 (Fig. 7B). Most elements in the gray zone are immobile, but C increased and both K and H decreased. Using a density ratio of 0.91, the calculated volume change in the gray zone is

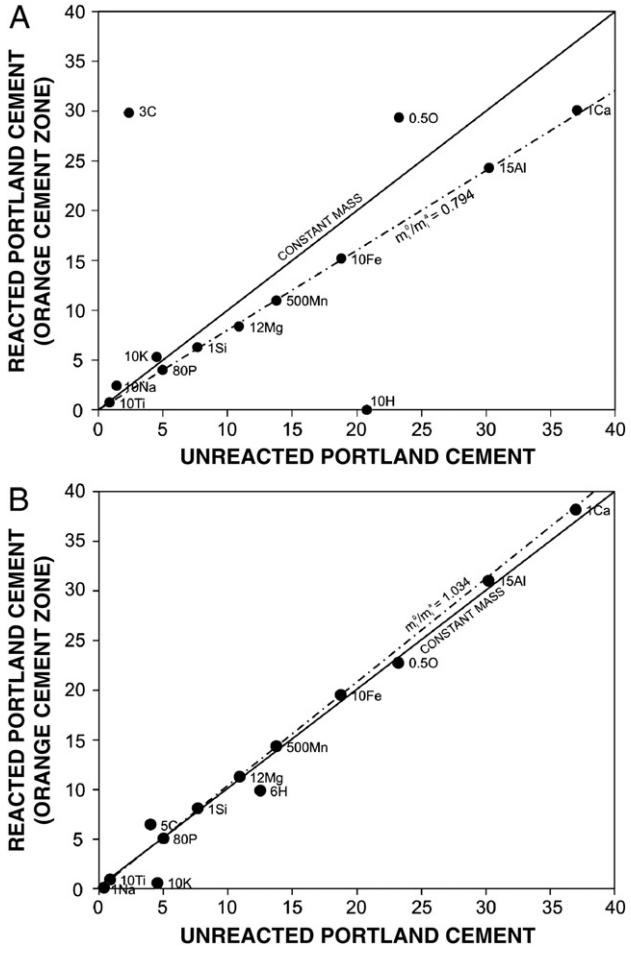

Fig. 7. ISOCON diagram for change in chemical composition from Portland cement before the experiment to the altered orange (A) and gray (B) cement zone. Related analyses for the major elements in weight percentage are shown in Table 1. Only the major elements were used for the ISOCON diagram. Best-fit ISOCON calculations for the orange and the gray zone resulted in slopes of 0.794 (m_i^0/m_i^a) and 1.034 (m_i^0/m_i^a) respectively. The numbers associated with the chemical symbols are scale factors. Scale factors other than 1× are indicated for the various species: for oxides, units are wt.%, for elements ppm. Solid line with slope of 1.0 defines a reaction at constant mass.

−9.04%. This apparent decrease in volume appears unrealistically large (e.g., significant stress fractures were not observed). In the calculation this occurs because there is only a small change in concentration with a rather large increase (10%) in density.

For an assumed constant volume the changes in elemental composition in the two altered cement zones are given in Table 3. With the exception of Mg and H, minor to negligible additions for almost all major elements took place in the orange zone. Larger additions are calculated for C and O (12.16 and 29.69%, respectively). The trace elements Zn, Rb, Sr, and Ba were added to the orange zone during the alteration process. The net result for the components listed in Table 3 is a mass gain of +17.28% relative to original Portland cement. Assuming constant volume, H decreased of about 0.26% in the grey zone, whereas 0.63% C and 4.18% O were added during the alteration process. In addition, some of the major and trace elements show different behavior and small losses of Na, K, and Zn took place in the gray zone. The net result is a negligible mass gain of 0.04% in the gray zone.

Changes in major and trace elements for the illite-rich shale were also calculated using the ISOCON method developed by Grant (1986). Fig. 8 shows the results of these calculations. The slope of the best-fit ISOCON for the altered shale yields (m_i^0/m_i^a) = 0.9618 and thus a mass increase of +3.98%. The change in density was not measured (the shale sample was a powder) and therefore a change in volume cannot be calculated. In the altered shale, degrees of enrichment or depletion of nearly all major elements are relatively small or within the calculated error. The distributions of elements in the ISOCON diagram for the altered shale (Fig. 8A) shows that nearly all major elements (Al, Ti, P, Si, Mg, Fe, and Ca) are relatively immobile, whereas LOI (lost on ignition), Mn, and Na contents slightly increased. Considering the results of the XRD analysis the increase in LOI could be a result of the formation of kaolinite. The changes in the trace element contents are in all cases related to leaching processes (Fig. 8B). Trace elements having immobile behavior during the reaction with $SCCO_2$ were Mo, Be, As, Pb, Hg, Zn, Sb, and U. Some of the trace elements such as Th, Tl, Rb, Sr, Cu, Li, Cs, Se, and in a lesser extent Ba were mobilized during the experimental study as demonstrated by a decrease in their concentrations. Kharaka et al. (2006) and Wigand et al. (2008) related the mobilization of trace elements to the precipitation and dissolution of iron and manganese oxyhydroxides. Hydrous iron oxide, a ubiquitous secondary mineral in aquifer sediments, has a very high specific surface area (around 600 $m^2 \cdot g^{-1}$) and thus a very high adsorption capacity (Davis and Kent, 1990). Iron oxyhydroxides incorporate elements such as P, Sr, Pb, U, Bi, Th, Y, and REE; whereas manganese hydroxides preferentially accumulate Co, Ni, Cu, Zn, Cd, Mo, Tl, and W. (Dubinin and Uspenskaya, 2006). The precipitation of manganese hydroxides could have been occurred in the shale due to the increase of Mn and LOI (Fig. 8B) but, if occurred, had no significant influence on the concentrations of trace elements such as Ni, Cu, Zn, Cd, and Tl. A breakdown of a Mn-bearing mineral phase in the cement could be the source of the Mn because the enrichment of Mn in the shale is consistent with the depletion of Mn in the cement. The immobile

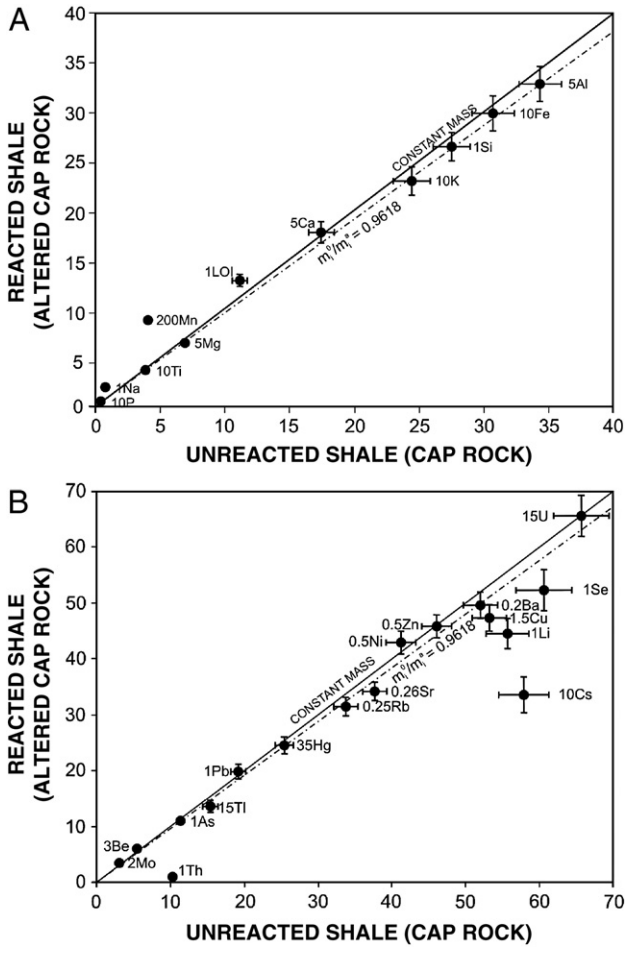

Fig. 8. ISOCON diagram based on U2-E1-IS and U3-E1-S1 shale compositions. (A) shows the changes in the major element and L.O.I. and (B) in the trace element composition. Scale factors other than 1× are indicated for the various species: for oxides, units are wt.%, for elements ppm. Solid line with slope of 1.0 defines a reaction at constant mass.

behavior of Fe excludes the formation of iron oxyhydroxides. This is also supported by the immobile behavior of arsenic. Under oxidizing and mildly reducing conditions, arsenic concentrations are usually controlled by adsorption, not mineral precipitation (Clement and Faust, 1981). Arsenic is strongly adsorbed to iron minerals (e.g., Masscheleyn et al., 1991). The depletion of alkali and earth alkali elements such as Li, Cs, Rb, Sr, and Ba in the shale could be seen as a result of the dissolution of calcite and ion-exchange mechanisms in clay minerals. In contrast to the highly reactive cement, reaction among shale, $SCCO_2$, and brine is limited to mobilization of a few trace elements, partial dissolution of calcite and albite, and formation of kaolinite. No evidence for reaction at the interface between shale and cement (e.g., no mineralization or discoloration) was observed. Thus, interaction between shale and cement in these experiments is minimal and may be limited to mobilization of trace elements out of the shale and into fluid that permeates the cement. These relationships are consistent with field observations (Section 4.4.) where no interaction is observed between cement and shale. Questions regarding processes that may occur at the interface between shale and cement will require additional experimental investigation and field study.

4.2. Geochemical modeling of fluid–rock–cement interactions in the experiment

To better understand precipitation of amorphous SiO_2 in the transition zone and interactions among $SCCO_2$, acidic brine, and basic cement, we consider aqueous SiO_2 (SiO_2(aq)) activity and pH during the different stages (Fig. 4) of the experiment. Without direct experimental measurement, a geochemical model is required to evaluate *in-situ* SiO_2(aq) activity ($a_{SiO2(aq)}$) and pH. We construct a reaction path geochemical model using Geochemist's Workbench 6.0.2 (Bethke, 2006) and the methods described in Section 3.2 and Table 2. Chemistry of starting brine and brine recovered from shale (Table 2) and mineralogy of shale and cement before and after reaction in the experiment (Table 1) were used as input parameters for the model.

At the beginning of the experiment, the stage in which brine saturates shale (Fig. 4), the model determines $a_{SiO2(aq)}$ and pH for starting brine injected into the experiment at 54 °C and for brine after it reacts with shale. These two fluid compositions are plotted as points #1 ($\log a_{SiO2(aq)} = -4.7$ and pH = 4.3) and #2 ($\log a_{SiO2(aq)} = -3.1$ and pH = 4.6), respectively, in Fig. 9. Based on the non-published results of previous experiments, calculations for brine reacted with shale assume a bench pH of 7.

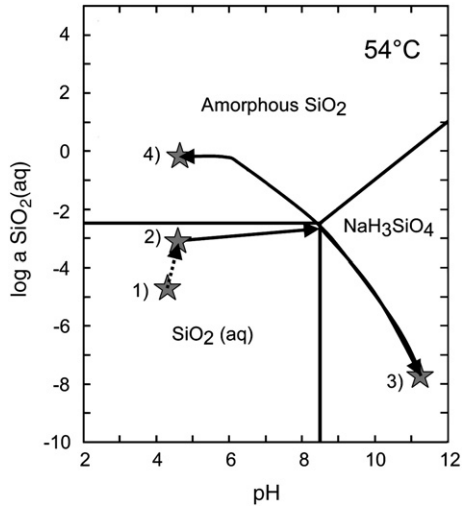

Fig. 9. $\log a_{SiO2(aq)}$ *versus* pH at 54 °C for the sequence of fluid–rock–cement interactions developed in the experiment. Numbered stars represent 1) brine before reaction with shale, 2) brine after reaction with shale, 3) brine after reaction with Portland cement, and 4) injection of $SCCO_2$ into reacted cement and brine. The calculations used Geochemist's Workbench 6.0.2 (Bethke, 2006), the thermodynamic dataset thermo.dat, and the B-dot ion association model. Chemistry of starting brine and brine recovered from shale (Table 2) and mineralogy of shale and cement before and after reaction (Table 1) were used as input parameters.

In the model, brine that has reacted with shale (point #2 in Fig. 9) is subsequently reacted with Portland cement. Relevant thermodynamic data are unavailable for many of the cement phases listed in Table 1, including alite, belite, brownmillerite, and amorphous C-S-H phases. Instead, a representative cement (16.2 wt.% portlandite, 4.3 wt.% larnite (Ca_2SiO_4), 1.5 wt.% rankinite ($Ca_3Si_2O_7$), 74.5 wt.% $Ca_2SiO_4 \cdot 7/6H_2O$, and 3.5 wt.% calcite) consistent with the original starting composition (Table 1) was used. Consequently, our geochemical model is not a rigorous thermodynamic rendering of the experiment but a qualitative evaluation of reaction trends and processes. Brine reaction with Portland cement increases fluid pH to approximately 11 and decreases $\log a_{SiO2(aq)}$ to −8.2 (point #3 in Fig. 9).

To represent $SCCO_2$ injection (Fig. 4), the model adds 0.9 M CO_2 to the ensemble of reacted cement and brine. This amount of CO_2 is sufficient to saturate brine at 54 °C and 19.9 MPa, as calculated with the Duan et al. (2006) equation of state. As a result of this process, pH decreases to 4.7, $\log a_{SiO2(aq)}$ increases to −0.2, and the brine becomes saturated with amorphous SiO_2 (point #4 in Fig. 9). The residual solid is comprised of 69% calcite, 11% dolomite and 20% amorphous SiO_2. This mineralogy compares favorably with the analyzed mineralogy of the orange zone of 43 wt.% calcite, 8 wt.% vaterite and 48 wt.% amorphous material (Table 1).

Our model suggests that multi-phase fluid–rock reactions among $SCCO_2$, brine, and Portland cement produce extreme pH fluctuations of ~6 pH units, from pH 4.6 in brine reacted with shale to pH 11 in brine reacted with cement to pH 4.7 once $SCCO_2$ is injected (Fig. 9). The model also predicts that SiO_2(aq) activity in brine decreases by water–cement reaction ($\log a_{SiO2(aq)}$ −8.2, point #3 in Fig. 9), wherein SiO_2 is locked in C-S-H phases in cement. SiO_2 is subsequently liberated once $SCCO_2$ is injected, providing a SiO_2 reservoir for subsequent precipitation of amorphous SiO_2 in the transition zone. Precipitates of amorphous SiO_2 at the interface between gray and orange zone cements are observed both in the experiment (Fig. 5) and in a field study of altered wellbore cement (Carey et al., 2007).

Our geochemical model explains how multi-phase fluid–rock reactions induce pH changes and mobilize SiO_2(aq) for precipitation of amorphous SiO_2 in the transition zone. However, as an equilibrium model constructed with a reaction path geochemical code, the model does not provide a mechanism for physical growth of the transition zone. Is the location and thickness of the zone controlled by initial penetration of brine or by subsequent supply of H_2O for reaction? Does growth of the zone require communication with flow in the fracture via some type of feedback loop? What is the minimum thickness of amorphous SiO_2 required for an efficient seal? Key questions of this nature require additional modeling using reactive transport codes, building on the foundation our experiments and model provide.

4.3. Relationship between the increase in flow and the opening of the fracture over time

Observations of the cement core after the experiment led to the proposition that the increase in flow over time is fracture related. A substantial quantity of CO_2 could not have migrated through the gray zone in the center of the two half cylinders from the fracture because highly reactive cement phases, such as portlandite and C-S-H, persist in this zone. Limited reaction of the gray zone with CO_2 is consistent with the idea that H_2O saturated CO_2 infiltrated the cement from within the fracture, carbonating the orange zone and forming a

transition zone between the orange and gray zones (Fig. 5). Precipitates of amorphous SiO_2 at this interface (Fig. 5) were responsible for the decrease in permeability and avoided further intrusion of H_2O saturated $SCCO_2$ into the gray cement. Similar observations were made by Carey et al. (2007) during the study of an altered wellbore cement recovered form the Kelly Snyder Field in western Texas.

Additional evidence for flow of $SCCO_2$ and/or $SCCO_2$-saturated brine along the fracture is the calcite precipitation along fracture surfaces. During exposure to H_2O saturated $SCCO_2$, approximately 1500 calcite crystals with an average volume of 248.8 μm^3 per mm^2 precipitated on both surfaces of the fractured cement core (Fig. 3D). Evaluation of SEM micrographs indicates that the fracture has been mineralized and filled with calcite along part of its length, but also has openings from 2.8 to 56.7 μm in width.

The opening of the fracture may be related to the growth of calcite at the fracture surfaces. Crystallization-induced stress during calcite precipitation depends on the supersaturation and the composition of the solution and could be as high as ~75 MPa (Wiltschko and Morse, 2001), a value approximately 3 times higher than the applied confining pressure.

4.4. Comparison with altered wellbore cements from EOR sites

Recently a core of wellbore cement was recovered from the Kelly Snyder Field of West Texas, a field with a 35 year history of $SCCO_2$ in enhanced oil recovery (Carey et al., 2007). Reaction among cement, $SCCO_2$ and formation water produced distinctive alteration zones in the core (Carey et al., 2007). The most striking zone is orange in color. It is 0.9 cm in width and contains calcite (44 wt.%), vaterite (33 wt.%), aragonite (8 wt.%), halite (13 wt.%), and quartz (2 wt.%) in addition to substantial amorphous material. This zone was interpreted by Carey et al. (2007) as carbonated cement. The orange-colored zone that formed in our experiment contains nearly the same amount of calcite as the orange zone of the cement core recovered from the Kelly Snyder field but contains less aragonite and vaterite (Table 1). Unlike the cement core from the Kelly Snyder Field, the orange zone that was formed during our experiment contains brownmillerite and a significantly higher fraction of X-ray amorphous phases. In normal cases the hydration of brownmillerite is a rapid process (less than 50 h, Drábik et al., 1988). At temperatures above 50 °C a hexagonal hydrate as a key precursor of the hydration is replaced by cubic hydrogarnet (Meller et al., 2004). Brownmillerite may have persisted in the experimental orange zone because $SCCO_2$ reacts primarily with hydrated cement phases (i.e., portlandite and C-S-H). The presence of alite, belite and brownmillerite in the experimental gray-colored zone, in which carbonation was less extensive than in the orange zone, suggests that infiltration of $SCCO_2$ did not dehydrate the hydrated cement phases (e.g., hydrogarnet).

A low permeable barrier of amorphous silica formed at the interface of the orange and gray zones in both the core recovered from the field and in our experiment (Fig. 5). Geochemical modeling (Fig. 9) suggests that this interface formed from reaction of C-S-H phases with the brine–$SCCO_2$ mixture. Other authors (e.g., Short et al., 2001) also concluded that amorphous SiO_2 forms during decomposition of C-S-H phases. We conclude that SiO_2(aq) and NaH_3SiO_4 forms during the decomposition of C-S-H. The stability of SiO_2(aq) and NaH_3SiO_4 depends on log $a_{SiO2(aq)}$ and the pH of solution (Fig. 9).

5. Summary and conclusions

In the present experiment, Portland cement reacts with H_2O saturated $SCCO_2$ and hydrated cement phases such as portlandite and C-S-H, forming calcite, aragonite, and vaterite. The molar volume of each of these $CaCO_3$ polymorphs is larger than that of portlandite, and the carbonation process resulted in a decrease in porosity. This may have led to the closing and/or blocking of pores and fractures, impeding the ingress of reactant, $SCCO_2$, and the egress of reaction product, H_2O. Reaction of C-S-H phases were the likely source of silica for amorphous silica precipitate that formed along the CO_2-reaction front in altered cement, probably reducing permeability and preventing further chemical reaction with H_2O saturated $SCCO_2$. The shift from alkaline to acidic pH due to cement–brine reactions and subsequent cement–brine–CO_2 carbonation reactions first liberates then immobilizes this silica. Reaction between hydrated cement phases and H_2O saturated $SCCO_2$ lead to euhedral calcite precipitation at the surface of a longitudinal fracture introduced in the cement. This mineralization led to opening of the fracture and a related increase in the permeability but was also observed to partially heal the fracture. The cement–$SCCO_2$–brine system was highly reactive whereas the shale–$SCCO_2$–brine system was not. No significant reaction occurred at the shale–cement interface in the experiment, an observation consistent with field observations. Calcite dissolution and kaolinite precipitation within the shale was due to shale–$SCCO_2$–brine reaction and not to interaction with the wellbore cement.

Acknowledgements

Funding was provided by Los Alamos National Laboratory (LDRD/DR) for this research and by the Department of Energy (LA-UR 08-0389). We would like to thank Steve Chipera for providing XRD analyses and Dale Counce for ICP-MS analyses. We also thank Melissa Fittipaldo for operating the SEM and EMP during our investigation. The authors are grateful to Emily Kluk for performing the XRF analyses and to Victor Medina for performing the porosity measurements. Bénédicte Ménez, Fabrice Brunet, Pascale Bénézeth and an anonymous reviewer provided constructive and detailed reviews of the manuscript.

References

Bethke, C.R., 2006. The Geochemist's Workbench Release 6.0: Reference Manual. University of Illinois, Urbana-Champaign, Champaign, Illinois.

Carey, J.W., Wigand, M., Chipera, S., WoldeGabriel, G., Pawar, R., Lichtner, P.C., Wehner, S., Raines, M., Guthrie, G.D., 2007. Analysis and performance of oil well cement with 30 years of CO_2 exposure from the SACROC field, West Texas, USA. Int. J. Greenh. Gas Control 1, 75–85.

Clement, W.H., Faust, S.D., 1981. The release of arsenic from contaminated sediments and muds. J. Environ. Sci. Health. Part A 16, 87–122.

Davis, J.A., Kent, D.B., 1990. Surface complexation modeling in aqueous geochemistry. Rev. Mineral. Geochem. 23, 177–260.

Drábik, M., Kaprálik, I., Oliew, G., Wieker, W., 1988. Conversion and heat evolution during hydration of aluminum and iron-containing clinker phases in presence of sulphates. J. Therm. Anal. 33, 679–684.

Duan, Z.H., Sun, R., Zhu, C., Chou, I.M., 2006. An improved model for the calculation of CO_2 solubility in aqueous solutions containing Na^+, K^+, Ca^{2+}, Mg^{2+}, Cl^-, and SO_4^{2-}. Mar. Chem. 98, 131–139.

Dubinin, A.V., Uspenskaya, T.Y., 2006. Geochemistry and specific features of manganese ore formation in sediments of oceanic bioproductive zones. Lithol. Miner. Resour. 41, 1–14.

Grant, J.A., 1986. The isocon diagram — a simple solution to Gresens' equation for metasomatic alteration. Econ. Geol. 81, 1976–1982.

Gresens, R.L., 1967. Composition–volume relationships of metasomatism. Chem. Geol. 2, 47–65.

Jacquemet, N., Pironon, J., Caroli, E., 2005. A new experimental procedure for simulation of H_2S + CO_2 geological storage — application to well cement aging. Oil Gas Sci. Technol. 60, 193–206.

Karl, T.R., Trenberth, K.E., 2003. Modern global climate change. Science 302, 1719–1723.

Kharaka, Y.K., Cole, D.R., Hovorka, S.D., Gunter, W.D., Knauss, K.G., Freifeld, B.M., 2006. Gas–water–rock interactions in Frio formation following CO_2 injection: implications for the storage of greenhouse gases in sedimentary basins. Geology 34 (7), 577–580.

Kutchko, B.G., Strazisar, B.R., Dzombak, D.A., Lowry, G.V., Thaulow, N., 2007. Degradation of well cement by CO_2 under geologic sequestration conditions. Environ. Sci. Technol. 41, 4787–4792.

Masscheleyn, P.H., Delaune, R.D., Patrick, W.H., 1991. Effect of redox potential and pH on arsenic speciation and solubility in a contaminated soil. Environ. Sci. Technol. 25, 1414–1419.

McLennan, S.M., Taylor, S.R., 1979. Rare earth element mobility associated with uranium mineralization. Nature 282, 247–250.

Meller, N., Hall, C., Jupe, A.C., Colston, S.L., Jacques, S.D.M., Barnes, P., Phipps, J., 2004. The paste hydration of brownmillerite with and without gypsum: a time resolved synchrotron diffraction study at 30, 70, 100 and 150 °C. J. Mater. Chem. 14, 428.

National Energy Technology Laboratory, 2002. U.S. National Brine Wells Database: U. S. Department of Energy, National Energy Technology Laboratory, unpaginated CD-ROM.

Pacala, S., Socolow, R., 2004. Stabilization wedges: solving the climate problem for the next 50 years with current technologies. Science 305, 968–972.

Regnault, O., Lagneau, V., Catalette, H., Schneider, H., 2005. Étude expérimentale de la réactivité du CO_2 supercritique vis-à-vis de phases minérales pures. Implications pour la séquestration géologique de CO_2. C.R. Geosci. 337, 1331–1339.

Short, N.R., Purnell, P., Page, C.L., 2001. Preliminary investigations into the supercritical carbonation of cement pastes. J. Mater. Sci. 36, 35–41.

Taylor, S.R., McLennan, S., 1985. The Continental Crust: its Composition and Crustal Evolution. Blackwell, Oxford. 312 pp.

Taylor, S.R., McLennan, S., 1995. The geochemical evolution of the continental crust. Rev. Geophys. 33, 241–265.

Wigand, M., Carey, J.W., Schuett, H., Spangenberg, E., Erzinger, J., 2008. Geochemical effects of CO_2 sequestration in sandstones under simulated in-situ conditions of deep saline aquifers. Appl. Geochem. 23, 2735–2745.

Wiltschko, D.V., Morse, J.W., 2001. Crystallization pressure versus “crack seal” as the mechanism for banded veins. Geology 29, 79–82.